Journal of Coastal Research	8	2	419–441	Fort Lauderdale, Florida	Spring 1992

Modeling of Hydrodynamics and Sedimentary Processes Related to Unbroken Progressive Shallow Water Waves

Georges Chapalain† and Barbara Boczar-Karakiewicz‡

†Institut de Mécanique de Grenoble
Grenoble, France

‡INRS-Océanologie
Université du Québec
Rimouski, Canada

ABSTRACT

CHAPALAIN, G. and BOCZAR-KARAKIEWICZ, B., 1992. Modeling of hydrodynamics and sedimentary processes related to unbroken progressive shallow water waves. *Journal of Coastal Research*, 8(2), 419-441. Fort Lauderdale (Florida), ISSN 0749-0208.

This paper reports on numerical modeling designed to examine hydrodynamics and sedimentary processes related to unbroken progressive waves propagating in nearshore areas. The first part of the paper concerns microscale processes developing in the near-bed boundary layer. At the first stage of the study a second-order turbulence closure model is applied. The numerical model is tested against experimental data and applied to the prediction of a near-bed flow of sediment in suspension induced by linear and nonlinear waves. For mild wave-dominated coastal environments with typically low volumetric sediment concentrations ($c = 10^{-3}$–10^{-4}) the model predicts a weak influence of sediment particles on the mean flow velocities. Therefore, at the second stage of the study, the modeling procedure is decoupled, separating the flow dynamics from diffusion and advection of sediment. A simpler, analytical closure model is applied and its results are tested against the second-order closure model, showing a satisfactory agreement. The second part of the paper is devoted to macroscale cross-shore processes. The simple analytical bottom boundary layer model is incorporated into the framework of a two-dimensional sediment transport and morphodynamical model of the outer shoreface of coastal zones subject to moderate-energy wind-dominated conditions.

ADDITIONAL INDEX WORDS: *Numerical model, bottom boundary layer, sand transport, longshore bars.*

INTRODUCTION

Wave-dominated coastal zones are dynamic regions where fluid motion extends down to the sea floor and interacts with bottom sediment. These interactions between waves and bottom sediment are extremely complex, ranging from microscale processes such as ripple formation or sediment-laden near-bed boundary layer flow to macroscale phenomena such as formation of longshore bedforms.

Sediment transport induced by waves over sandy rippled beds subject to erosion is complex on account of the turbulent motion of the fluid and the formation of vortices which inject localized bursts of sediment into the near-bed flow. Resulting sediment suspension is observed to be highly variable in space and time (INMAN and BOWEN, 1962; DOWNING, 1984; HANES and HUNTLEY, 1986; HANES, 1990; HANES *et al.*, 1988; VINCENT *et al.*, 1991) influencing the wave-induced sediment fluxes.

In the present study, the first and main objective is a description of a wave-induced near-bed boundary layer flow over rippled beds subject to erosion composed of non-cohesive sediment. First, the boundary layer flow is described by a second-order turbulence closure model originally proposed by SHENG (1985, 1986) and SHENG and VILLARET (1989). Later, the same model is used for testing simplified decoupled procedures for the hydrodynamics (JOHNS, 1970) and for the diffusion and advection of sediment (HUNT, 1954; NIELSEN, 1979, 1988).

Given the extreme complexity of a general coastal model, no attempt is made here to model completely nearshore fluid and sediment dynamics. At present, efforts are being made to develop three-dimensional models of the nearshore flow field (see for example HORIKAWA, 1988; SVENDSEN and LORENZ, 1989) but these particularly complex and expensive models still require further field testing before it will be possible to incorporate sediment transport successfully. The part of the present work devoted to macroscale processes concerns only wave fields, wave-induced sediment transport and topographical changes seawards of the breakpoint on gently sloping sand outer shorefaces (of the order of one per cent or less) for the

91032 received 1 April 1991; accepted in revision 18 November 1991.

specific case in which the depth contours are straight parallel, the wave trains are normally incident, weakly nonlinear, and relatively long, and the wave-induced motion is intense enough so that the near-bed boundary layer is turbulent. Because the modeling applies to gently sloping offshore topography, researchers tend to neglect the effect of directly incident reflected (CARTER *et al.*, 1973) waves. In addition, the present modeling does not incorporate standing cross-shore infragravity waves, which may influence the flow field, particularly in inner parts of the shoreface (BOWEN and INMAN, 1971). Under these special conditions, which are however relevant to processes occurring on natural beaches, we adopt a nonlinear model for the evolution of the wave field in the shoaling region that is based on sloping bottom Boussinesq-type equations (PEREGRINE, 1972). Another important limitation of the model is that the mechanism for shoaling transformations consists of nonlinear interactions between the first and second harmonics of a purely progressive wave train (LAU and BARCILON, 1972; BOCZAR-KARAKIEWICZ *et al.*, 1987).

Laboratory experiments and observations of outer shorefaces show that their temporal topographical changes are slow (several thousands of wave periods) compared to the rapid changes in the fluid flow (BOCZAR-KARAKIEWICZ *et al.*, 1987; SHIELS, 1986). On account of this stability, it is therefore permissible to apply a two-step time-loop procedure in the development of the macroscale morphodynamical model. In the first step, local microscale properties of the bottom boundary layer flow and of the related sediment flux pattern are calculated over a bed topography which is instantaneously fixed. In the second step of the modeling procedure, the temporal evolution of macroscale bedforms is calculated with constant parameters of the fluid flow and of the related sediment flux.

The resulting morphodynamical model is applied to two different wave-dominated shorefaces, one from a lacustrine environment, the other from a marine environment.

MODELING OF WAVE-INDUCED NEAR-BED BOUNDARY LAYER PROCESSES

A Second-Order Turbulent Closure Model

Presentation of the Model

The governing equations for the near-bottom flow with suspended sediment are simplified by several assumptions. Following LUMLEY (1978) it is assumed that the suspended sediment concentration is sufficiently low to neglect particle interactions, but high enough to represent the mixture as a continuum. Although the fluid is Newtonian in its clear state, it is however not obvious that it will remain Newtonian in the presence of suspended particles. It is therefore assumed that the smallest length scales of the turbulence are large in comparison to the largest particle sizes (BARENBLATT, 1953). The inertia of the particles is assumed to be small and thus the sediment velocity is equal to the fluid velocity minus the particle fall velocity w_f. The sediment is assumed to be composed of uniform quartz spheres ($\rho_s = 2.65$).

Completing the previous assumptions by Boussinesq's formulation of the Reynolds shear stress and the turbulent mass flux, the sediment-laden flow may be approximately described by the following system of equations

$$\frac{\partial u}{\partial t} = -\frac{1}{\rho_f}\frac{\partial p}{\partial x} + \frac{\partial}{\partial z}\left(\nu_t \frac{\partial u}{\partial z}\right) \tag{1}$$

$$\frac{\partial c}{\partial t} = w_f \frac{\partial c}{\partial z} + \frac{\partial}{\partial z}\left(\gamma_t \frac{\partial c}{\partial z}\right) \tag{2}$$

$$\rho = \rho_s c + (1 - c)\rho_f \tag{3}$$

where u denotes the horizontal fluid velocity inside the boundary layer, p is the pressure, c is the volumetric suspended sediment concentration, ρ is the density of the fluid-sediment mixture with ρ_f and ρ_s denoting respectively the fluid and sediment density; ν_t and γ_t are respectively the eddy viscosity and diffusivity.

In the one-dimensional advection-diffusion equation (2) horizontal diffusion has been ignored. However, at the edge of sand clouds the horizontal gradient of concentration is large and may cause a significant lateral diffusion. Given the complexity of the problem we simply accept this simplification which is partly justified by HANES and HUNTLEY's (1986) recent field measurements about time lags between suspension events suggesting that vertical gradients in sediment flux are greater than horizontal gradients.

The closure of the set of equations (1), (2), and (3) is achieved by adding equations quantifying the turbulent kinetic energy q^2 and the turbulent macroscale Λ (SHENG, 1985, 1986; SHENG and VILLARET, 1989).

These equations are supplemented by two analytical expressions for the eddy viscosity ν_t and for the eddy diffusivity γ_t resulting from a local "quasi-equilibrium" approximation which is valid when the time scale of mean flow is much greater than the time scale of turbulence Λ/q (LEWELLEN, 1977). The equations for q^2 and Λ, and the expressions for ν_t and γ_t are defined in Appendix A.

The solution of the global system of equations (1), (2), and (3) and (A.1) and (A.2) must satisfy boundary conditions at the upper and lower limit of the boundary layer. Such a solution may be obtained when it is assumed that inside the boundary layer the flow is fully turbulent and that the boundary layer thickness is large in comparison to the scale of the bed roughness so that there is a significant region inside the boundary layer which from the hydrodynamic point of view is not directly affected by the details of the individual roughness elements.

In the following numerical calculations the solution extends from the bed to a distance of ten times the JONSSON (1978) characteristic length scale δ_I,

$$\delta_I = 0.074\,(a_b k_b)^{1/2} \tag{4}$$

where a_b is half the near-bed orbital extension defined in Appendix B and k_b is the bed roughness height which is estimated using GRANT and MADSEN's (1982) empirical model

$$k_b = 27.7 h_r h_r/\lambda \tag{5}$$

where h_r and h_r/λ are respectively the height and steepness of ripple also defined in Appendix B.

The boundary conditions at the upper limit of the above defined boundary layer require

(i) the mean horizontal velocities u to match the free stream velocity just outside the bottom boundary layer U_b, expressed as a Fourier series

$$u = U_b = \tfrac{1}{2}\left|\sum_j U_{bj}\exp\left[j(\omega_j t - \varphi_j)\right] + \text{c.c.}\right| \tag{6}$$

where ω_j and φ_j are respectively the wave pulsation and the phase of the jth harmonic component, and c.c. stands for the complex conjugate of the quantity just preceeding it.

(ii) the vanishing of all turbulence-related characteristics of the water-sediment mixture comprising

- the suspended sediment concentration: $c \rightarrow 0$,
- the turbulent eddies scaled by the macroscale: $\Lambda \rightarrow 0$,
- the turbulent kinetic energy: $q^2/2 \rightarrow 0$.

At the lower limit of the boundary layer it is required

(i) to provide an estimation of the near-bed shear stress τ_b given by the following expression

$$\tau_b = \rho\,|u^*|\,u^* \tag{7}$$

where u^* denotes the friction velocity obtained when it is assumed that the near-bed velocity follows a logarithmic law in a region close to the boundary (JONSSON, 1963, 1966; JONSSON and CARLSEN, 1976; LAMBRAKOS, 1982; GRANT *et al.*, 1983; HINO *et al.*, 1983; SUMER *et al.*, 1986; SLEATH, 1987).

(ii) to estimate the near-bed flux of sediment particles into the suspension,

$$\gamma_t \left.\frac{\partial c}{\partial z}\right|_{z=0} = p(t) \tag{8}$$

where p(t) denotes Svendsen-Nielsen's pick-up function defined in Appendix B (B.4)

(iii) that the function describing the turbulent macroscale length Λ, which follows the logarithmic law inside the boundary layer, tends asymptotically to a linear function when approaching the bottom, which imposes:

$$\Lambda = \alpha_c z, \tag{9}$$

where α_c is a constant related to von Karman's constant K, $\alpha_c = 2K(2)^{1/2}$

(iv) the turbulent energy flux across the bed to vanish,

$$\frac{\partial q^2}{\partial z} = 0 \tag{10}$$

In all presented results of numerical calculations the bottom friction coefficient has been estimated for simplicity using JONSSON's (1978) semi-empirical model

$$\begin{cases} f_w = \dfrac{0.0605}{\mathrm{Log}^2 \dfrac{27\delta_I}{k_b}} & k_b/a_b < 1 \\[2ex] f_w = 0.24 & k_b/a_b > 1 \end{cases} \tag{11}$$

where δ_I, k_b and a_b are respectively the above defined JONSSON length (4), the roughness

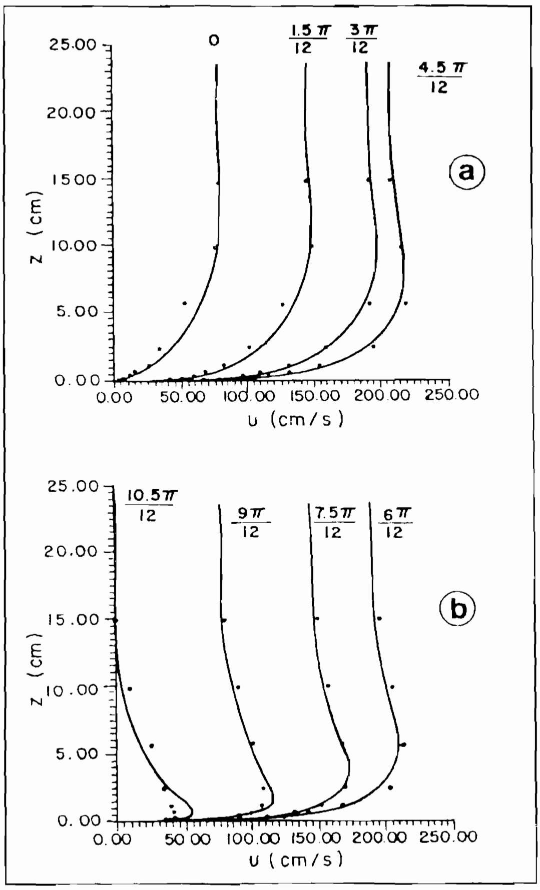

Figure 1. Predicted and measured mean velocity profiles. (a) Acceleration phase. (b) Deceleration phase. Solid curves, predicted profiles. Solid circles, data from Sumer *et al.* (1986).

height and half of the near-bed orbital excursion (*cf.* Table 1, Appendix B).

Numerical solutions of the formulated boundary layer problem were obtained by using the standard finite-difference method originally suggested by SHENG (1985). The uncentered two-time level scheme yields finite-difference equations solved by a classical "up-down" variant of Gaussian elimination algorithm. In a staggered numerical grid the mean variables (u, c, ρ) are calculated at one half-level, while the turbulent quantities (q, Λ, ν_t, γ_t) are computed at the other half-level. The number of time-steps per wave-period were chosen to be greater than or equal to 200. The height of $\delta = 10\ \delta_1$ was discretized by some 100 steps. The overall convergence of the solution has

Table 1. *Ripple characteristics (from Grant and Madsen, 1982).*

	Equilibrium Phase $(\psi'/\psi'_c) < (\psi'/\psi'_c)_B$	Breakup Phase $(\psi'/\psi'_c) > (\psi'/\psi'_c)_B$
h_r/a_b	$0.22(\psi'/\psi'_c)^{-0.16}$	$0.48S_*^{0.8}(\psi'/\psi'_c)^{-1.5}$
h_r/λ	$0.16(\psi'/\psi'_c)^{-0.04}$	$0.28S_*^{0.6}(\psi'/\psi'_c)^{-1.0}$

been tested by comparing the distributions of different variables in consecutive wave-cycles. The rate of convergence depends slightly on the variable considered. Generally, convergence was fully achieved after twenty cycles.

Numerical Experiments

(a) Clear Water Case. In the following stage, the formulated bottom boundary layer model will be tested experimentally against the set of data obtained by SUMER *et al.*, (1986) using a laser-Doppler velocimeter in clear water. On account of the degree of sophistication of these recent measurements which involve both mean and turbulent velocities, the comparison is expected to be more complete than SHENG's (1984, 1986) validation based on mean horizontal velocity measurements performed by JONSSON and CARLSEN (1976). The orbital velocity and the motion period are equal to 210 cm/sec and 8.12 sec respectively. The measured value of the roughness height is $k_b = 0.38$ cm.

Figure 1 presents a comparison of calculated and measured mean flow profiles in accelerating (Figure 1a) and decelerating (Figure 1b) phases. These profiles display the two classical behaviors of oscillatory boundary layers: the "overshoot" occurring at the time of the maximum free stream velocity and the differences in the flow field between the two stages of favourable (Figure 1a) and adverse (Figure 1b) pressure gradients. Globally, these results indicate that the model is able to reproduce fairly well the experiment except when the flow reverses. This discrepancy seems to be a consequence of using throughout the whole wave-cycle a fully turbulent bottom friction law for a flow which is in fact laminar around flow reversals. In Figure 2 are depicted the turbulent kinetic energy profiles. At almost every phase they appear to be composed of a lower and an outer region. The lower region (z < 8 cm) characterized by high values is the place where most of the turbulent energy is created. In the outer part of the boundary layer (z > 8 cm), where little tur-

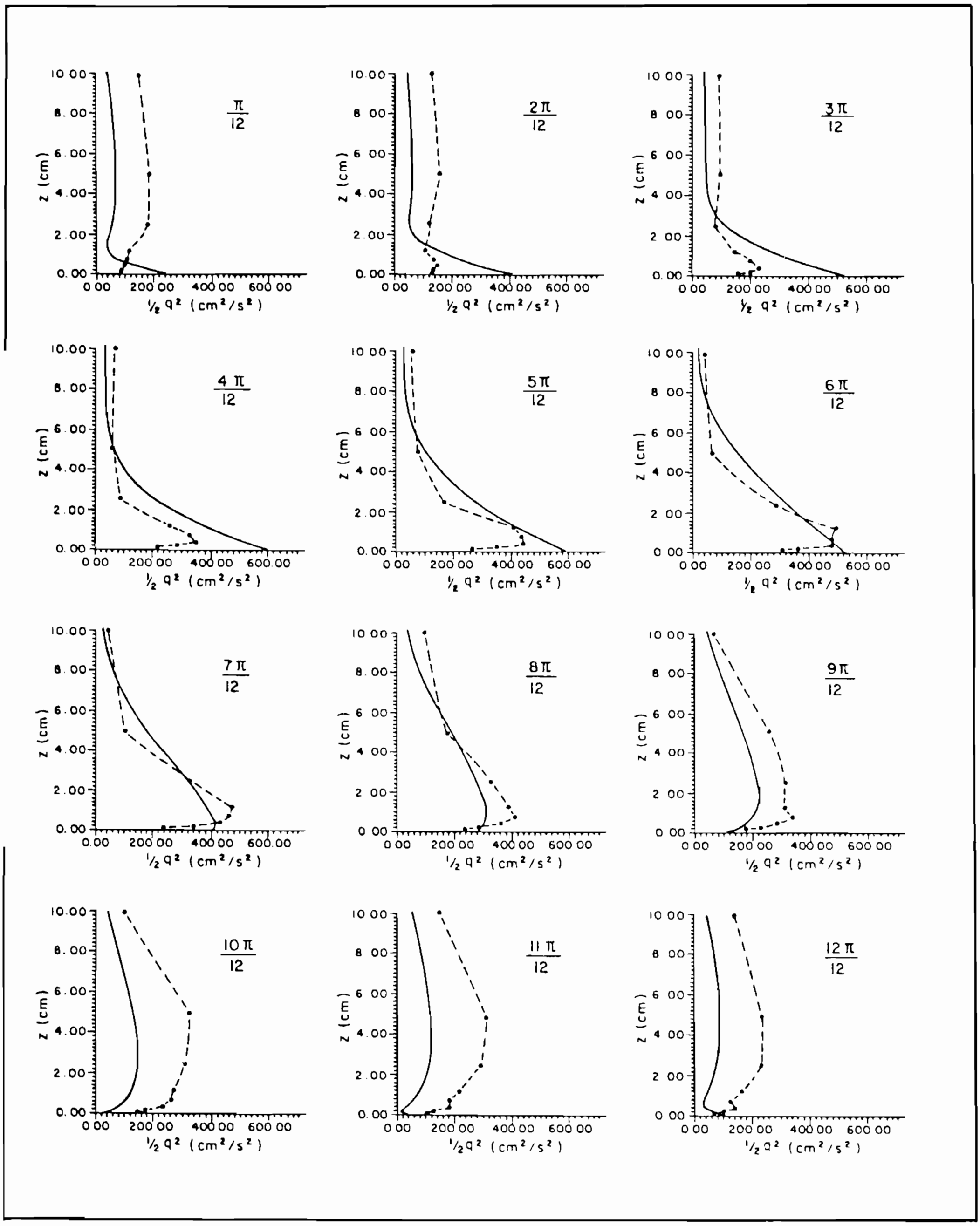

Figure 2. Predicted and measured turbulent kinetic energy profiles. Solid curves, predicted profiles. Dashed curves, data from Sumer *et al.* (1986).

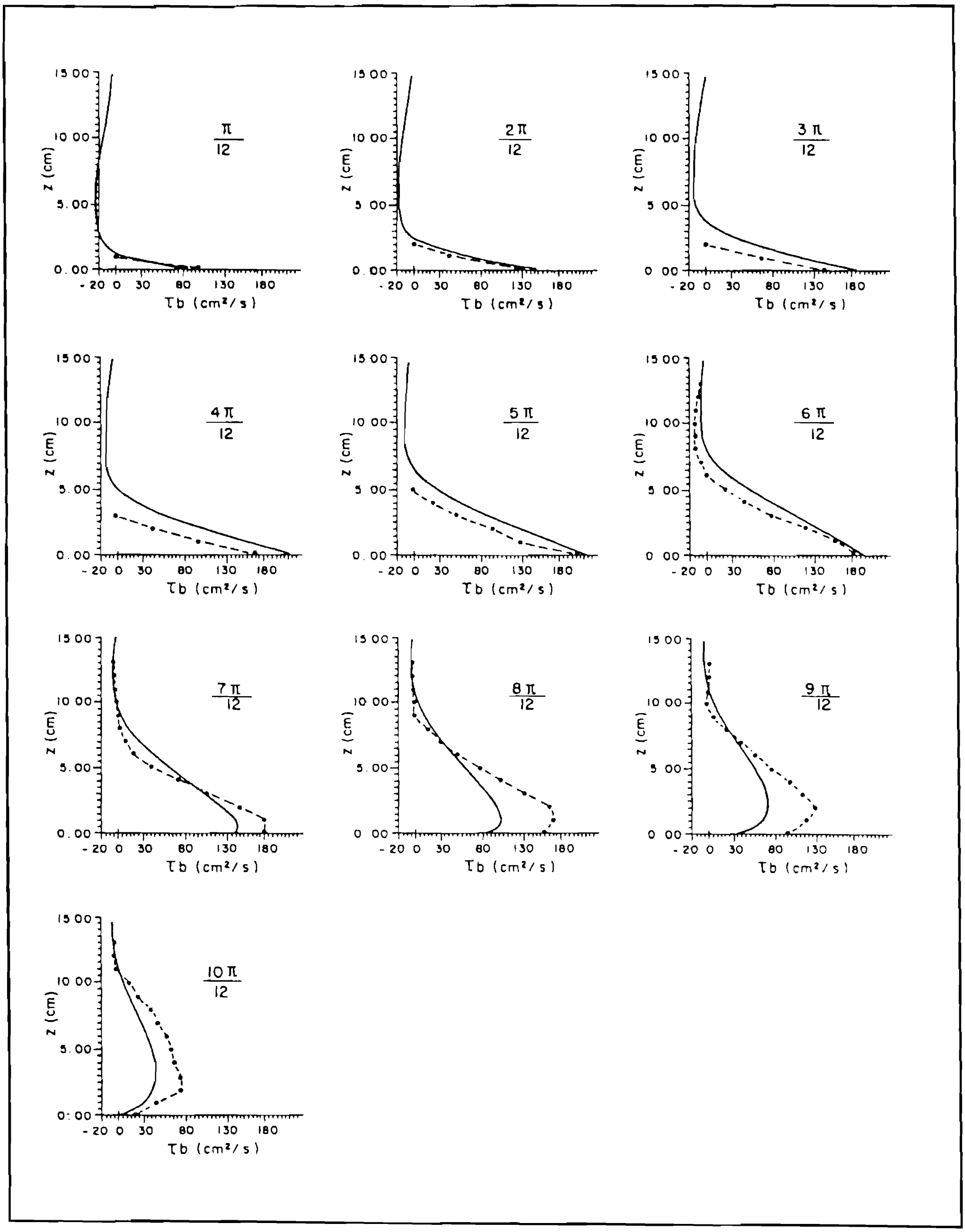

Figure 3. Predicted and measured shear stress profiles. Solid curves, predicted profiles. Dashed curves, data from Sumer *et al.* (1986).

bulent energy is generated, the kinetic energy tends to much lower and almost constant values. The turbulent energy varies with phase angle in the cycle and also displays phase shifts increasing with the distance from the bed and resulting from an upward spread of turbulence by diffusive processes. Figure 2 shows that turbulence in accelerating and decelerating phases is different as observed experimentally (HAYASHI and OHASHI, 1983; HINO *et al.*, 1983). Moreover, we notice that the model is able to yield fairly good agreement with data, except around flow reversal. In Figure 3 instantaneous calculated and measured shear stress profiles are plotted. As for the turbulent velocity, we observe two different regions: a near-bed region with high shear stress values and an outer layer where shear vanishes. Once again, as for the turbulent velocity, the complex spatio-temporal shear stress pattern reveals spatially varying phase shifts and differences between accelerating and decelerating phases. Particularly in the accelerating phase close agreement between numerical and experimental results is observed. Later, in the decelerating phase the shear stress near the bottom is somewhat overpredicted by the model. This discrepancy between theory and experiment was also found by JUSTESEN (1988) who used a classical k-ϵ-model of turbulence.

(b) Sediment-Laden Near-Bed Flow Case. The computations are concentrated on a quantitative analysis of the adjustment of localized sediment bursts injected into the lower part of the boundary layer to the ambient flow within the upper part of the layer. It also is intended to estimate the influence of the concentration gradient of suspended sediment particles on the boundary layer flow characteristics. On account of the lack of complete experimental data on sediment-laden boundary layer flow the study is restricted to numerical results.

Computations are performed for sinusoidal and asymmetrical (cnoidal), regular and monochromatic wave trains corresponding to typical coastal conditions (wave period T_t = 10 sec, wave amplitude a = 0.25 m, water depth H = 5 m). In both cases the wave energies are taken to be identical.

The movable bed is assumed to consist of fine sand with uniform grain diameter d = 0.3 mm. This corresponds to a critical wave-extended Shields parameter defined in Appendix B and equal to $\psi'_c = 0.35$. According to GIBBS *et al.*'s (1971) experimental formula (B.5) the fall velocity w_f is equal to 0.05 m/sec. The roughness thick-

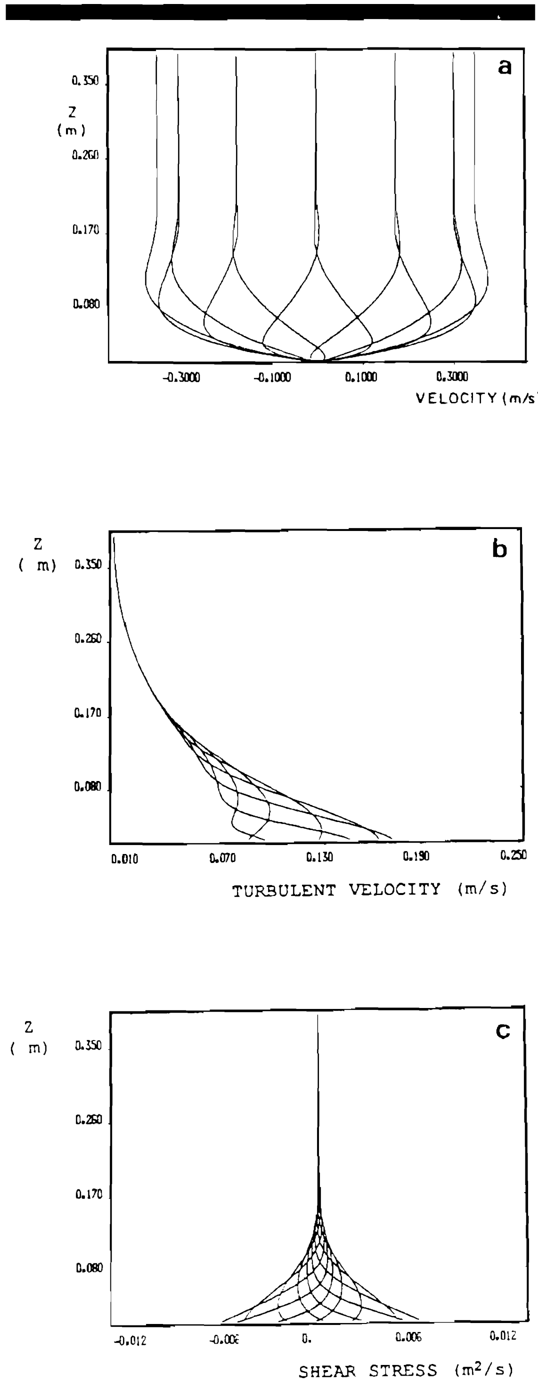

Figure 4. (a) Mean velocity profiles, (b) turbulent velocity profiles, and (c) shear stress calculated by the second-order turbulence closure model under the typical sinusoidal wave defined in the text. The profiles are shown in increments of 30°.

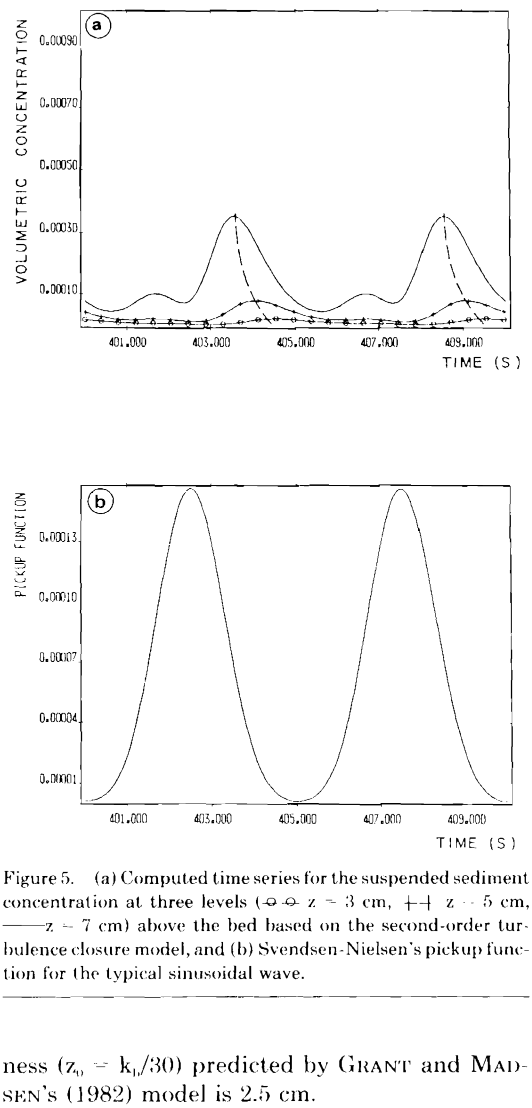

Figure 5. (a) Computed time series for the suspended sediment concentration at three levels (-o-o- z = 3 cm, +-+ z = 5 cm, —— z = 7 cm) above the bed based on the second-order turbulence closure model, and (b) Svendsen-Nielsen's pickup function for the typical sinusoidal wave.

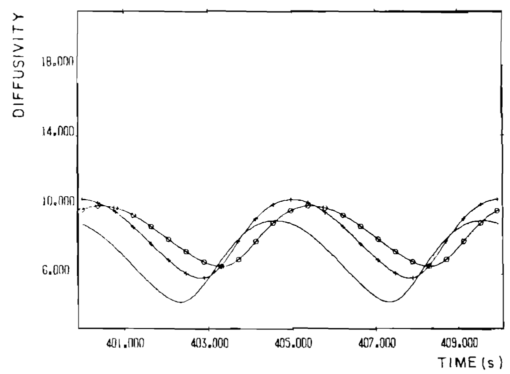

Figure 6. (a) Computed time series for the diffusivity under the typical sinusoidal wave at three levels (-o-o- z = 3 cm, +-+ z = 5 cm, —— z = 7 cm) above the bed based on the second-order turbulence closure model.

ness ($z_0 = k_b/30$) predicted by GRANT and MADSEN's (1982) model is 2.5 cm.

In the case of a sinusoidal wave (such as U_{b1} = 0.35 m/sec and U_{b2} = 0) the first-order orbital velocities, the turbulent velocities and the shear stress are presented in Figure 4 for every 30° of the wave cycle. The predicted spatial and temporal variability of the turbulent quantities shows similarities with the earlier analysed experimental results of SUMER *et al.*, (1987).

The pick-up function (B.4) for a symmetrical sinusoidal wave provides two identical near-bed bursting events (Figure 5b). Resulting time-dependent sediment concentration calculated at three standard levels (z = 3, 5, 7 cm) is shown in Figure 5a. They exhibit a phase shift in the distribution of local extrema of the predicted sediment concentration. The phase shift increases with the distance from the bottom, which reflects the effect of vertical sediment diffusion. Another notable feature of the predicted concentration is a very strong temporal variability controlled by depth- and time-dependent diffusion γ_t (A.4) (Figure 6).

The influence of periodic, localized bursts of sediment on the mean boundary layer flow is analysed by comparing results for a sediment-laden fluid and for water with no sediment.

Instantaneous profiles of the mean velocity for the sediment-laden flow (solid line in Figure 7) and for water without sediment (dashed line in Figure 7) show surprisingly little difference, even in the lowest part of the boundary layer where the sediment concentration is relatively high.

In the case of asymmetrical waves such as U_{b1} = 0.34 m/sec and U_{b2} = 0.084 m/sec, the sediment suspension shown in Figure 8a appears to be highly asymmetrical as a consequence of an asymmetrical near-bed sediment supply provided by an asymmetrical pick-up function (Figure 8b). Sediment concentration predicted by the model and observations (see also KENNEDY and LOCHER, 1972) show a satisfactory qualitative agreement with a special capability of the model to reproduce secondary peaks around flow reversals (Figure 8a, 9). Comparisons of instantaneous first-order horizontal velocities for a sediment suspension and water without any sediment show the same tendency as presented earlier for the case of sym-

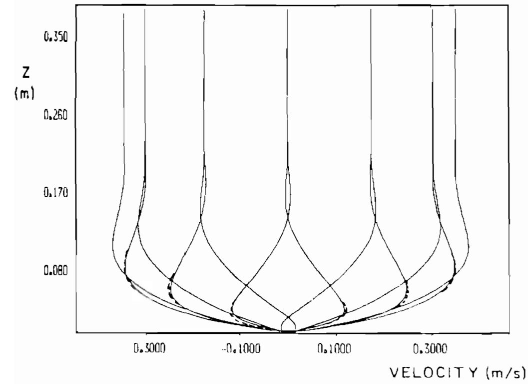

Figure 7. Computed mean velocity profiles under the typical sinusoidal wave based on the second-order turbulence closure model with (solid curve) and without (dashed line) suspended sediment.

metrical sinusoidal waves: a weak influence of sediment particles on the boundary layer dynamics.

A Decoupled First-Order Closure Model

Conclusions resulting from numerical experiments using a second-order turbulent closure model justify a simplification of the modeling procedure for a flow with a low sediment concentration. In this procedure, the flow dynamics and the sediment concentrations are modelled separately.

The hydrodynamics of the wave-induced boundary layer flow are now described by an analytical approach proposed by JOHNS (1970) using the following Reynolds averaged momentum equation

$$\frac{\partial u}{\partial t} + u\frac{\partial u}{\partial x} - \frac{\partial u}{\partial \eta}\int_0^\eta \frac{\partial u}{\partial x}\,d\eta = \frac{\partial U_b}{\partial t} + U_b\frac{\partial U_b}{\partial x} + \frac{1}{l^2}\frac{\partial}{\partial \eta}\left[\nu_t\frac{\partial u}{\partial \eta}\right] \qquad (12)$$

where $\eta = z/l$ and l is a characteristic length scale of the boundary layer.

The required eddy-viscosity closure was obtained by applying a simple time-independent model

$$\nu_t = [U]\cdot[L] \qquad (13)$$

where [U] and [L] are characteristic scales for the velocity and turbulent eddies respectively.

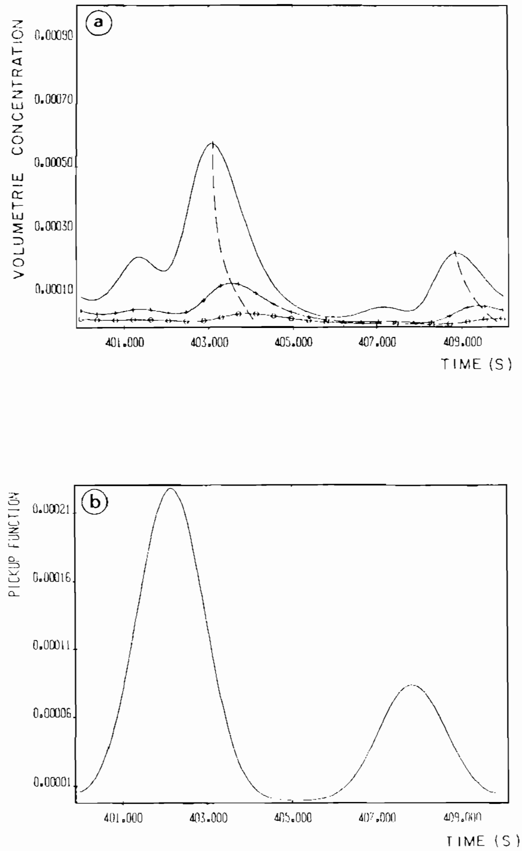

Figure 8. (a) Computed time series for the suspended sediment concentration at three levels (o o z = 3 cm, + + z = 5 cm, ——z = 7 cm) above the bed based on the second-order turbulence closure model, and (b) Svendsen-Nielsen's pickup function for the typical asymmetric wave.

The velocity scale [U] is estimated by the friction velocity

$$u^* = \sqrt{\frac{\tau_{bm}}{\rho}} \qquad (14)$$

where τ_{bm} denotes the maximum bottom stress and the length scale [L] in (13) is assumed to be the ripple height (NIELSEN *et al.*, 1982).

A classical perturbation analysis (JOHNS, 1970) provides explicit expressions for the first- and second-order horizontal mean velocity. Both expressions are defined in Appendix C.

The predicted velocity profiles are shown in Figure 10 for every 30° of the wave cycle. Com-

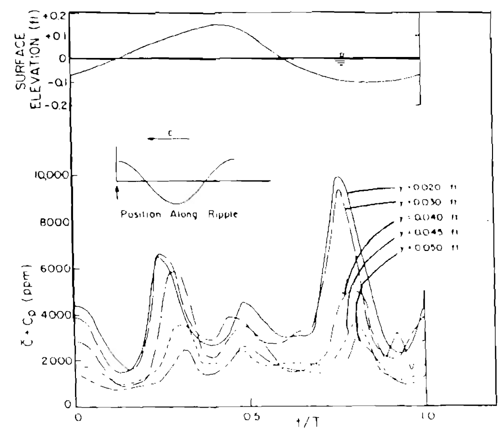

Figure 9. Measured temporal variation of the suspended sediment concentration above a rippled bed submitted to an asymmetric oscillatory flow (from BHATTACHARYA and KENNEDY, 1971).

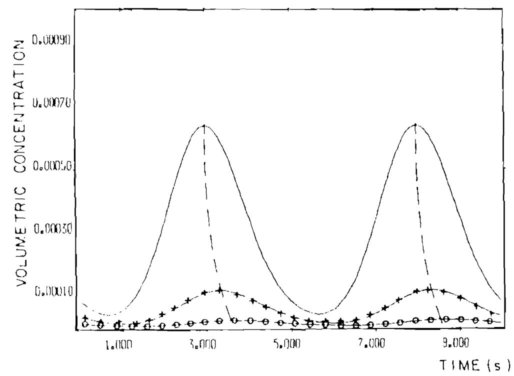

Figure 11. (a) Computed time series for the suspended sediment concentration under the typical sinusoidal wave at three levels (z = 3 cm, z = 5 cm, z = 7 cm) above the bed based on the constant, time-independent eddy viscosity model.

parison with results of the second-order turbulent closure model (Figure 4) shows a satisfactory agreement.

A simple analytical model can now be derived to predict the sediment concentration in a wave-induced near-bed boundary layer flow.

The time-periodic and modally decomposed (NIELSEN, 1979, 1988) sediment concentration c,

$$c = \sum_n c_n \exp(in\omega_1 t)\,\zeta_n(z) \qquad (15)$$

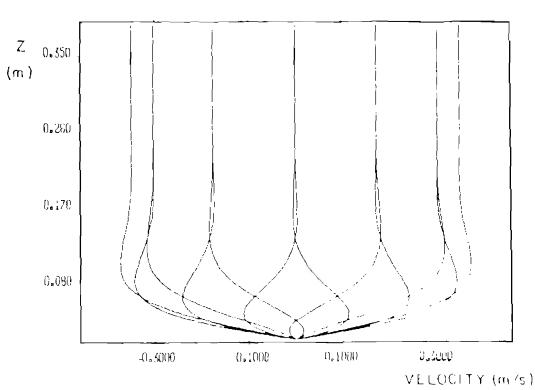

Figure 10. Mean velocity profiles (calculated by the constant, time-independent eddy viscosity model) under the typical sinusoidal wave.

is assumed to satisfy the advective-diffusive equation (10) and the following boundary conditions:

- at the upper part of the boundary layer, where the concentration tends to zero, and consequently $\zeta(z) \to 0$ for $z \to \infty$
- at the lower part of the boundary layer the concentration tends to the quantity predicted by the pick-up function (defined in Appendix B, B.4).

According to the proposed model the spatial and temporal sediment concentration is described by an explicit analytical expression c(X, z, t) (expressed in the Appendix C, C.4). In this expression the eddy diffusivity γ_t is assumed to be proportional to the eddy viscosity (HUNT, 1969; SMITH and McLEAN, 1977; RODI, 1980, 1987) and is evaluated by requiring the sediment to be confined only into the turbulent bed boundary layer,

$$\bar{C} = 0.05\,\bar{C}_0 \quad \text{at } z = \delta \quad \text{and} \quad X = 0 \qquad (16)$$

Predicted sediment concentrations for both sinusoidal and asymmetrical waves are presented in Figures 11 and 12. The simple model correctly reproduces the depth-dependent phase shift at the location of the local sediment extremal (Figure 13). However, when a locally constant eddy diffusivity is used, the temporal part of the predicted sediment concentration follows the pattern imposed by the near-bed concentration described by the pick-up function.

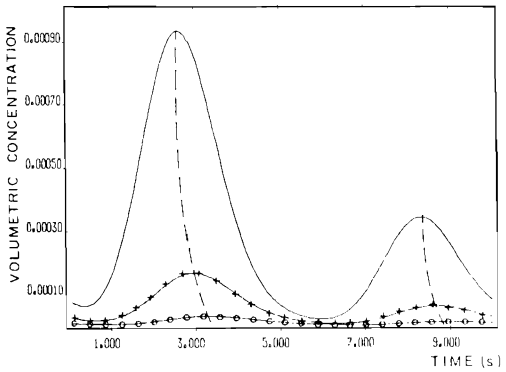

Figure 12. (a) Computed time series for the suspended sediment concentration under the typical asymmetric wave at three levels (-o-o- z = 3 cm, -+-+ z = 5 cm, —— z = 7 cm) above the bed based on the constant, time-independent eddy viscosity model.

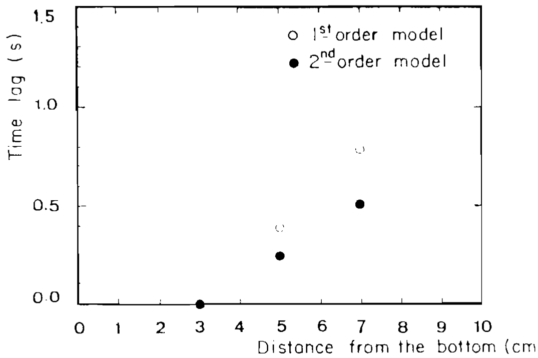

Figure 13. Computed time lag of peak concentrations between different levels. Solid circles, second-order turbulence closure model. Open circles, constant, time-independent eddy viscosity or first-order turbulence closure model.

Local Cross-Shore Sediment Transport Rate

Observations and numerical experiments show that sediment movement over a rippled bed occurs mainly as suspension in vortices shed from the ripple crests. The bed load occurring during a fraction of the wave cycle contributes to the transport in "feeding" these vortices (HORIKAWA, 1981, 1988; SHIBAYAMA and HORIKAWA, 1982).

Therefore, in the present model the wave-induced, time-averaged sediment transport rate Q is estimated by the product of the instantaneous sediment concentration and the sediment velocity vector

$$Q = \frac{1}{T}\int_0^T \int_0^\delta u(z,t)c(z,t)\,dz\,dt \qquad (17)$$

In order to analyse the quantitative contributions of time-independent and time-dependent flow velocities and concentrations to the sediment transport rate Q, the product u.c. in (17) will be formally decomposed

$$u(z,t)\cdot c(z,t) = |\alpha u^{(1)}(z,t) + \alpha^2\beta\,|u_s(z) + u_p^{(2)}(z,t)||\cdot[\bar{C}(z) + c(z,t)] \qquad (18)$$

where $u^{(1)}$ and $u_p^{(2)}$ denote the first- and second-order periodic velocity components, u_s is the time-averaged velocity, $\bar{C}$ denotes the mean concentration and c is the instantaneous concentration.

In the following we separate the local sediment flux Q into two components

$$Q = Q_m + Q_n \qquad (19)$$

where Q_m denotes the contribution of time-independent quantities and Q_n the contribution of time-dependent quantities.

The component Q_m is

$$Q_m = \frac{S}{T}\int_0^\delta \bar{C}(z)\cdot u_s(z)\,dz \qquad (20)$$

where S controls the threshold of sediment movement and is defined by

$$S = \begin{vmatrix} 0 & \text{if } \psi' < \psi'_c \\ 1 & \text{if } \psi' > \psi'_c \end{vmatrix} \qquad (21)$$

where ψ' and ψ'_c are respectively GRANT and MADSEN's (1982) wave-extended Shields parameter and its critical value (see Appendix B).

Choosing now for the mean sediment concentration in (18) the following expression (ROUSE, 1937)

$$\bar{C}(z) = \bar{C}_0\exp(-Dz) \qquad (22)$$

with

$$D = w_f/\gamma_t$$

and substituting in (17) the mass transport velocity defined in Appendix B, the component Q_m may also be expressed by an explicit formula given in Appendix C. Note that this expression is valid

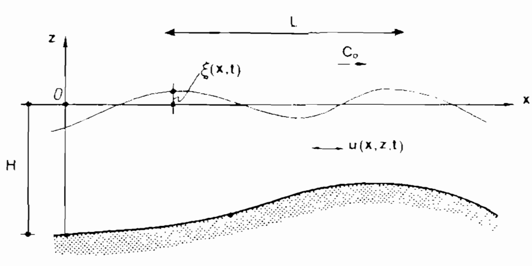

Figure 14. Sketch of definitions used.

for a flow field restricted to its first two harmonic components ($j = 1, 2$).

Proceeding now in a similar way with time-dependent quantities in (18), the component Q_n may also be made explicit and the related expression is given in Appendix C.

MODELING OF MACROSCALE PROCESSES

Limitations and Assumptions

Before going further, it is necessary to present and discuss the limitations and assumptions of the macroscale modeling. The present modeling concentrates on gently sloping outer shorefaces (of the order of one per cent or less) that are composed of uniform grain size sediments and that are subject to moderate normally incident progressive water-waves. The inviscid flow field model assumes that the bathymetric profile has plane-parallel contours and that no energy is reflected or dissipated (except by friction inside the near-bed boundary layer). The nonlinear model for the evolution of the wave field in the shoaling region is based on sloping bottom Boussinesq-type equations that contain terms accounting for weak dispersion due to finite depth, and weak nonlinearity due to finite amplitude. A further bold simplification of the model is that the mechanism for shoaling transformations consists of nonlinear interactions between the first and second harmonics of a purely progressive wave train (LAU and BARCILON, 1972; MEI and UNLUATA, 1972; MEI, 1983; BOCZAR-KARAKIEWICZ *et al.*, 1987; CHAPALAIN *et al.*, in press).

A Simple Water-Wave Model

Presentation of the Model

The incident regular two-dimensional wave train is characterized by an amplitude a and a wavelength L. It propagates in a domain described by a coordinate system (x, z) and shown in Figure 14. The undisturbed water level is at $z = 0$ and $h(x)$ is the water depth at point x. The vertical deviation from equilibrium of the free surface at point x at time t is $\xi(x, t)$ and $q(x, t)$ is the depth-averaged horizontal velocity. All physical variables are non-dimensionalized and scaled:

$$h = \frac{\bar{h}}{H}, \quad x = \frac{\bar{x}}{H}, \quad t = \frac{\bar{t}}{\sqrt{H/g}}$$

$$\xi = \frac{\bar{\xi}}{\alpha H}, \quad q = \frac{\bar{q}}{\alpha\sqrt{gH}} \tag{23}$$

where H represents a characteristic depth, g is the acceleration due to gravity, and $\alpha = a/H$ is a relative wave amplitude parameter.

The set of Boussinesq equations describing the shallow water wave is modified by a dissipative term induced by the bottom shear stress of the underlying turbulent boundary layer:

$$q_t + \xi_x + \alpha q q_x = \frac{h^2}{3} q_{xxt} + h h_x q_{xt} + \frac{1}{2} h h_{xx} q_t - \frac{R}{h} q \tag{24}$$

$$\xi_t + [(\alpha\xi + h)q]_x = 0 \tag{25}$$

In the derivation of the dissipative term $(R/h)q$ it has been assumed that friction is linear (MEI, 1983), where the constant R,

$$R = \frac{4}{3\pi} f_w \alpha q_{max} \tag{26}$$

is expressed by constant flow and friction parameters: the depth-averaged maximum velocity q_{max} at $x = 0$, and JONSSON's (1978) friction coefficient f_w (11).

Following LAU and BARCILON (1972) and BOCZAR-KARAKIEWICZ *et al.* (1987) we seek a solution of (23) and (24) where the free surface elevation ξ is represented by a simple Fourier series limited to its two first components

$$\xi = \xi(x, X, t)$$

$$= \frac{1}{2}\left|\sum_{j=1}^{2} a_j(X)\exp[i(k'_j x - \omega_j t)] + c.c.\right| \tag{27}$$

The first-order amplitudes a_j in equation (27) are taken to vary on the scale of wavelengths, and therefore depend on X, which is a horizontal length-scale measured in wavelength L. That is, $X = \bar{x}/L = \beta x$, where $\beta = H/L$ is the aspect ratio for the motion assumed to be of the order of α. A similar representation is postulated for q.

In equation (27) ω_1 is the frequency of the postulated incoming wave train, $\omega_2 = 2\omega_1$ is its second harmonic and k'_1 and k'_2 are wave numbers associated with ω_1 and ω_2, respectively.

It is further assumed that the principal features of the bottom variation are gradual, and therefore, it also may be taken that h is a function h(X) of the long variable, only (*i.e.* $h(X) = 1 + O(\alpha)f(X)$ where f is an O(1) function).

The dispersion relation results from first-order linear theory and reads

$$k'^2_j = k_j^2 + i\frac{R\omega_j}{1 - \dfrac{\omega_j^2}{3}} \tag{28}$$

where k_j denotes the first-order wave numbers obtained when friction is ignored.

The amplitudes ξ, and consequently the depth-averaged velocities q, result from solvability conditions for the second-order approximation (Lau and Barcilon, 1972)

$$\begin{cases} a_{1X} + H_1(X)a_1 \\ \quad + S_1(X)\exp\left(\dfrac{\Delta k^I X}{\beta}\right)\exp\left(-i\dfrac{\Delta k^R X}{\beta}\right)a_1 a^*_2 = 0 \\ a_{2X} + H_2(X)a_2 \\ \quad + S_2(X)\exp\left(\dfrac{\Delta k^I X}{\beta}\right)\exp\left(i\dfrac{\Delta k^R X}{\beta}\right)a_1^2 = 0 \end{cases} \tag{29}$$

where * denotes complex conjugate, $\Delta k' = \Delta k^I + i\Delta k^R = k'_2 - 2k'_1$ and H_1, H_2, S_1 and S_2 are known functions of X defined in Appendix D.

As shown in equations (28) and (29), the essential modifications induced by a linear friction term (Equation 26) appear in the first-order dispersion relation (Equation 28). The nonlinear set of equations (29) for the amplitudes a_j ($j = 1, 2$) remains identical when compared to the frictionless model (see Lau and Barcilon, 1972; Boczar-Karakiewicz *et al.*, 1987), except that in all coefficients the frictionless wave number k_j has to be replaced by k'_j (see appendix D).

For a chosen frequency ω_1 of the incident wave the set of equations (29) has to be completed by the values at the seaward boundary X = 0. These values can be extracted from field measurements or given by a larger scale wave model including intermediate water.

The coupled system of nonlinear evolution equations (29) supplemented by the boundary conditions are solved numerically using a stable and accurate fourth-order Runge-Kutta method (Boczar-Karakiewicz *et al.*, 1987).

Table 2. *Model-input data and related non-dimensional quantities for the typical wave-dominated environment run.*

$T = 10s$	$d = 0.35$ mm		
$a = 0.25$ m	$\rho_s = 2.65$	slope = 0.04%	$0 < X < 8$
$H = 5$ m	$w_f = 0.05$ ms^{-1}		
$\omega_1 = 0.449$	$\psi'_c = 0.032$		
$\alpha = 0.050$			
$\beta = 0.074$			

When a_1 and a_2, and thereby ξ and q are determined, the "bottom boundary layer driving" fluid velocity at the bed U_b may be obtained from q (Peregrine, 1972) and expressed by the following formula

$$U_b(x, X, t) = \frac{\alpha}{2}\left\{\sum_{j=1}^{2}\left(1 - \frac{\beta^2 h^2 k'^2_j}{6}\right)\left(\frac{\omega_j}{k'_j}\right) \cdot a_j(X)\exp[i(k'_j x - \omega_j t)] + c.c.\right\} \tag{30}$$

A Numerical Experiment

To illustrate the properties of the model, a numerical experiment with a set of typical wave parameters in coastal environments considered earlier ($T_1 = 10$ sec, a = 0.25 m, H = 5 m) is carried out over a plane beach profile (1 in 250 slope) (Figure 15c). Here, we arbitrarily take $a_1(0) = 1$ and $a_2(0) = 0$. The friction coefficient is taken equal to 0.24. This value comes from semi-empirical results which will be presented in detail in the forthcoming section. For information, this estimation assumes that the bottom is made of sand particles of diameter d = 0.35 mm and is covered with ripples. Table 2 summarizes the model-input data and the related non-dimensional quantities. A typical instantaneous wave profile normalized by the characteristic wave amplitude (a) is shown in Figure 15b. Note that the typical wave profiles, the amplitude of which are enormously exaggerated in comparison to the horizontal scale, become progressively more complex as they propagate into shallower water. Figure 15a shows the spatial evolution of the first two harmonic amplitudes a_j

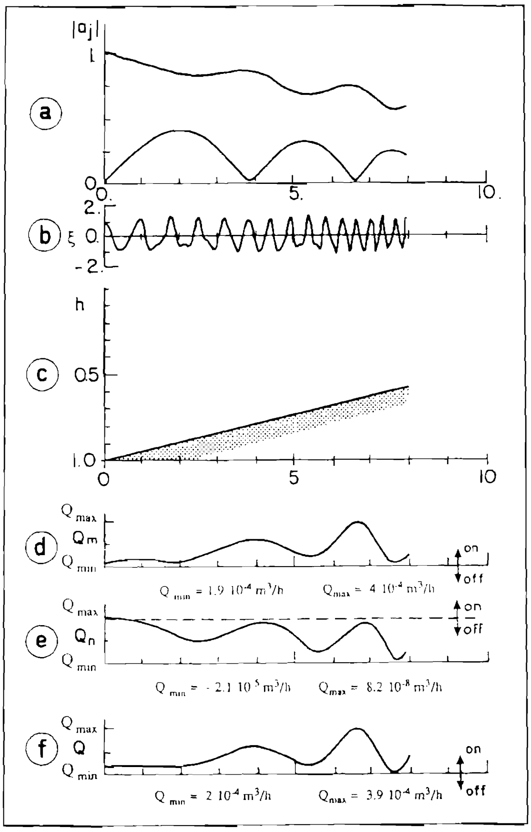

Figure 15. Model predictions. (a) Two first harmonic component amplitudes non-dimensionalized by the wave amplitude. (b) Free surface elevation at a given time non-dimensionalized by the wave amplitude. (c) Nearshore bathymetry non-dimensionalized by the incident water depth. (d) Time-independent sediment transport rate Q_m. (e) Time-dependent sediment transport rate Q_n. (f) Total sediment transport rate Q. The horizontal distance X is measured in incident wavelengths.

normalized by the characteristic wave amplitude which exhibits the well-known (GODA, 1967; GALVIN, 1968; MEI and UNLUATA, 1972; BOCZAR-KARAKIEWICZ, 1972; BENDYKOWSKA, 1975; CHAPALAIN *et al.*, in press) nonlinear interaction repetition length L_T which appears to decrease with local water depth. Note also the differential reduction of each harmonic component which tends to balance the wave shoaling (Figure 15b).

Macroscale Pattern of the Cross-Shore Sediment Transport Rate

The local suspended sediment transport rate has been derived earlier (Appendix C). We will now apply this estimator to the calculation of the sediment transport rate in the cross-shore direction by using the cross-shore pattern of the driving velocity U_b. The results of the simulation for the above case study are shown in Figures 15d, e and f. Figures 15d, e and f display respectively the spatial evolution (normalized by the characteristic wave amplitude) of the time-independent contribution Q_m, of the time-dependent contribution Q_n and of the total sediment transport rate Q.

Comparisons of the results presented for $|a_j|$ and Q_m, Q_n and Q show that all these quantities oscillate in space on the same long horizontal scale, called the repetition length L_T. This distance, characterizing the surface wave has been defined as a distance between two successive maxima of the higher harmonic of ξ. The total sediment transport flux Q is directed shorewards, due to the predominant shorewards contribution of Q_m. In contrast, the time dependent term Q_n varies and provides locally a negative contribution to the sediment flux Q. In this experiment the quantity Q_n is of much lower magnitude than Q_m, but Q_n increases with increasing wave asymmetry.

Macroscale Bathymetrical Changes

In order to calculate the macroscale bathymetrical changes, we employ the conservation equation of sediment mass

$$-C_p \frac{\partial h}{\partial T} + \beta \frac{\partial Q(X)}{\partial X} = 0 \qquad (31)$$

where C_p the concentration of the compact bed is taken equal to 0.74, assuming an ideal rhomboedric arrangement of spherical particles within the bed (RAUDKIVI, 1976; DYER, 1986) and T is a slow time variable consistent with the observed stability of the outer shoreface bathymetry.

A straightforward Euler method is used to solve (31) and get the configuration at time T = ΔT. This procedure may be then reiterated to compute an updated bed profile at 2ΔT, 3ΔT and so on.

Figure 22 shows results obtained from a numerical experiment, where all components of the morphodynamical model are linked together. The same model-input data as above are considered. The final state of the bed topography calculated after twenty slow time-steps (Figure 16c) represents a set of shore-parallel, periodic bars exhibiting a spacing of the bars intimately connected

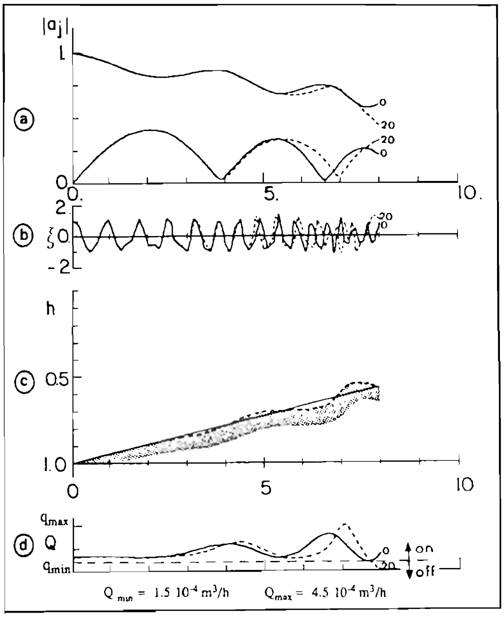

Figure 16. Initial and final model predictions. (a) Two first harmonic component amplitudes. (b) Free surface elevation at a given time. (c) Nearshore bathymetry. (d) Total sediment transport rates.

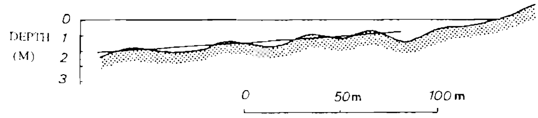

Figure 17. Observed longshore bars on the shoreface of Wasaga Beach, Ontario, Canada.

with the repetition length L_T in the wave field (Figure 16a and b) and in the sediment transport rate (Figure 16d). In parts of the bed configuration where the divergence of the sediment transport rate is negative, erosion occurs forming the troughs of the bar system. Crests formed where the sediment transport rate is positive. Note that for a constant sediment transport rate, no changes in bed topography appear. Note also that, as the bed deforms in response to the wave regime, the relative mean energy in the second harmonic amplitude increases progressively as the wave train propagates into shallower water (Figure 16a).

In spite of the numerous simplifying assumptions, we will now try to test the proposed morphodynamical model in the context of natural wave-dominated environments. Direct comparisons of the predictions of the model will be made with two measured outer shorefaces that feature a classical array of longshore sand bars, one from a lacustrine environment and one from a marine environment.

The marine case study application concerns Wasaga Beach located along the shore of Georgian Bay in Lake Huron. On account of its location in a narrow bay which is part of a bounded water body this area is hydrodynamically very simple with waves whose period and height are respectively about 5 sec and 0.25 m propagating exclusively from the North. The bathymetric survey of the outer shoreface displays a mean bottom profile whose slope is about 0.5%. This mean profile is modulated by four well-developed shore-parallel periodic bars characterized by a crest-to-crest distance that decreases as the water depth decreases (Figure 17). This known mean profile will be used as initial profile in the morphological modeling. Granulometric analysis reveals a mean grain size of approximately 0.35 mm. With the above defined wave regime the friction coefficient f_w evaluated using JONSSON's (1978) model is found equal to 0.24 all over the foreshore profile. Table 3 summarizes the model-input data and the related non-dimensional quantities. Since information is lacking on the seaward boundary conditions, and because the present morphodynamical model is only a conceptual model, the boundary values of the harmonic components are arbitrarily taken equal to $a_1(0) = 1$ and $a_2(0) = 0$. In addition, the origin has been chosen under these conditions so as to form the outer bar crest at the correct observed location. The outcome of the numerical experiment is displayed in Figure 18. The simulation is performed over twenty time-steps. The evolution of the initially featureless sloping bed is shown in Figure 18c. An initial and a final in-

Table 3. *Model-input data and related non-dimensional quantities for Wasaga Beach run.*

$T = 5s$	$d = 0.35$ mm		
$a = 0.11$ m	$\rho_s = 2.65$	slope = 0.5%	$0 < X < 8.5$
$H = 1.7$ m	$w_f = 0.05$ ms^{-1}		
$\omega_1 = 0.533$	$\psi'_c = 0.032$		
$\alpha = 0.065$			
$\beta = 0.089$			

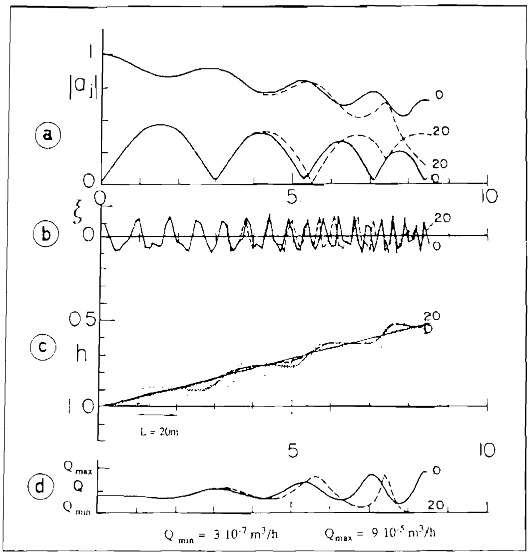

Figure 18. Prediction of the formation of a longshore bars system for the outer shoreface of Wasaga Beach. Initial (solid line) and final (broken line) model predictions. (a) Two first harmonic component amplitudes. (b) Free surface elevation at a given time. (c) Calculated bathymetry and measured bathymetry (dotted line). (d) Sediment transport rates.

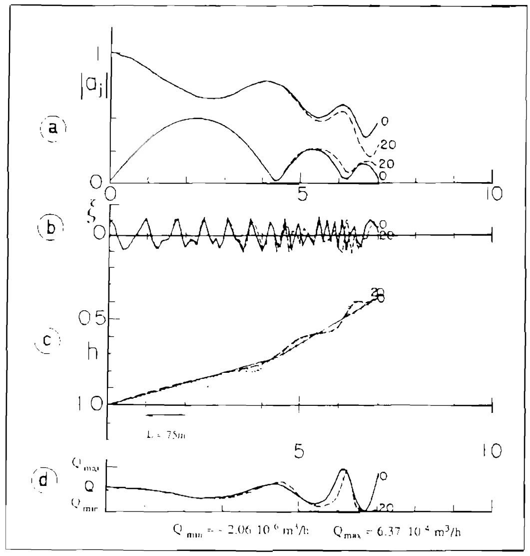

Figure 20. Prediction of the formation of a longshore bars system for the outer shoreface of Stanhope Lane Beach. Initial (solid line) and final (broken line) model predictions. (a) Two first harmonic component amplitudes. (b) Free surface elevation at a given time. (c) Calculated bathymetry and measured bathymetry (dotted line). (d) Sediment transport rates.

stantaneous wave profile are depicted in Figure 18b. As for the previous simulation (Figure 16), the increase in the relative mean energy in the second harmonic amplitude as waves propagate into shallower water becomes more pronounced as the bed deforms in response to the wave regime. The properties of the bar system (number of bars, crest-to-crest distance) appear to be fairly well predicted by the model. Nevertheless, it appears from the results that the amplitude of the external bar predicted by the model is underestimated. The uncertainties of field measurements and the difficulty of selecting the initial bathymetric profile, combined with the crudeness of the present model, reduce the significance of this discrepancy. The time-scale over which bars form is found to be about three years. This estimation is in agreement with the observed long-term stability of the sedimentary features in this site (DAVIDSON-ARNOTT and PEMBER, 1980).

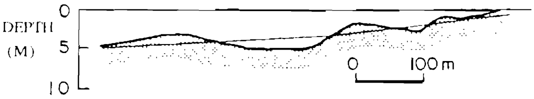

Figure 19. Observed longshore bars on the shoreface of Stanhope Lane Beach, P.E.I., Canada.

The second application in a marine environment is given by Stanhope Lane Beach located along the East coast of Prince Edward Island in the Gulf of St. Lawrence. During Fall 1984, an experiment (C2S2) was conducted on this beach, which is subject to a wave regime characterized by periods exceeding 10 sec. The measured bathymetric shoreface profile displays a mean bottom profile composed of two parts whose slopes are respectively about 0.35% and 0.75%. Additionally, it has three shore-parallel, periodic bars whose crest-to-crest spacing decreases with the water depth as pointed out earlier in the case of Wasaga Beach (FORBES *et al.*, 1986; Figure 19). The granulometric analysis suggests a mean sediment grain diameter equal to 0.35 mm. Table 4 summarizes the model-input data and the related non-dimensional quantities. Figure 20 shows the results of the model. As in the preceding simulation, the number of time-steps is equal to twenty. It appears again from these results that the calculated bottom evolution agrees fairly well with the observation, except for the amplitude of the external bar which is strongly underestimated by the model. In the present case, the time-scale of formation of the shore-parallel periodic bar system is about thirty years. The result confirms the observed stability of this outer shoreface profile (SHIELS, 1987).

Table 4. *Model-input data and related non-dimensional quantities for Stanhope Lane Beach run.*

$T = 12s$	$d = 0.35$ mm		0.35%	$0 < X < 4.4$
$a = 0.27$ m	$\rho_s = 2.65$	slope =		
$H = 4.1$ m	$w_f = .05\ ms^{-1}$		0.75%	$4.4 < X < 7$
$\omega_1 = 0.344$	$\psi'_c = 0.032$			
$\alpha = 0.065$				
$\beta = 0.056$				

CONCLUSIONS AND DISCUSSION

Complex interactions between the flow and the sandy bed take place in wave-dominated coastal areas. The present modeling incorporates a wide range of simplifying assumptions. While these assumptions are necessary due to complexity of actual coastal processes, it is hoped that they have some physical basis and the results of this conceptual modeling can suggest directions for future research.

The first step in the search of a better understanding of these interactions is the description of the microscale processes active in the unsteady intermittent sediment-laden near-bed flow. The present study shows that such a boundary layer flow may be described and analyzed using the second-order turbulence closure model of SHENG (1986) and SHENG and VILLARET (1989). Results provided by this boundary layer model indicate that for a low volumetric sediment concentration (typically $c = 10^{-3}$–10^{-4}) as obtained under moderate-energy wave conditions, the presence of sediment particles in the fluid does not influence significantly the dynamics of the flow, thus allowing decoupled modeling procedures to be applied. The second-order turbulence closure model has been applied to test a simple analytical decoupled model, based on the concept of constant eddy viscosity/diffusivity, which provides explicit expressions for the flow velocity, sediment concentration and sediment fluxes.

The present sediment transport model integrates the instantaneous vertical structure of the flow and of the suspended sediment concentration. It is an improvement over semi-empirical sediment transport models like SUNAMURA's (1980) model and also over most of the models which are based on BAGNOLD's (1963) energetics concept and which therefore use vertically-integrated equations. Consequently, these last models ignore the details of the vertical distribution of sediment flux. Moreover, they assume implicitly that the sediment transport responds to the near-bed water velocity in an instantaneous, quasi-steady manner. If this quasi-steady assumption is more or less valid for bedload transport, it appears unreasonable for suspended sediment transport (BAILARD, 1981).

The second step of the work consists of modeling the macroscale phenomena controlling surface wave dynamics, sediment transport and bathymetric response to wave action. In the elaboration of this macroscale modeling, available elements of sediment-laden bottom boundary layer flow developed in the first part of the paper are used to determine the cross-shore sediment transport pattern and the bathymetric changes.

Quantitative numerical experiments performed with this simple analytical model for a gently sloping outer shoreface show that sediment transport rate contributions due to time-dependent concentration and first-order orbital velocities are weak. In the outer part of the shoaling zone, the predominant sediment transport rate results from time-averaged boundary layer flow characteristics and is directed shorewards. However, the impact of time-dependent quantities increases significantly with increasing wave asymmetry.

The morphodynamical modeling resulting from the calculation of bathymetrical changes and resulting interactions between the wave field and the mobile sandy bed leads to a conceptual model for the formation of submarine shore-parallel, periodic bars. This model is tested against field measurements made in lacustrine and marine wave-dominated environments. In particular, the model predicts fairly well: (1) the bar number, (2) the bar spacing, and (3) the stability of these sedimentary features which is revealed by the long time-scale for formation of fully developed structures. This agreement between predictions and measurements is sufficiently good to warrant some confidence in the formative mechanism for outer longshore bars based on nonlinear shoaling of progressive wind-generated shallow water-waves.

Before concluding, it is necessary to discuss again some of the limitations of the present modeling. The bolder simplifying assumptions concern the second part of the study devoted to macroscale processes. They consist of:

(i) considering a two-dimensional weakly nonlinear and weakly dispersive water wave model based on Boussinesq-type equations for gently sloping bottom.
(ii) using a harmonic treatment of the primitive wave model limited to the two first components.
(iii) neglecting the effects of reflection, breaking processes, edge-waves, and standing cross-shore infragravity waves.

Some of these assumptions are more justified than others. The first and the last assumption restrict the application of the modeling to gently sloping outer shorefaces that are subject to relatively long, moderate waves propagating from a shore-normal direction on a bathymetric profile with plane-parallel contours. The second assumption is motivated by simplicity and cost considerations. Nevertheless, in order to defend or justify this assumption *a posteriori*, we recall that the major contribution to the total suspended sediment transport rate is imputable to the time-independent mass transport velocity and not to the first-order time-dependent harmonic components of the velocity. Extension of the modeling to other more sophisticated nearshore flow field models (especially the intermediate water wave model) is a logical step towards a more complete sediment transport and morphodynamical modeling. Note that these improvements can be made without affecting the principles of the global modeling, in particular:

(i) the spatial decoupling between the macroscale inviscid interior flow phenomena and the microscale turbulent near-bed boundary layer processes, and
(ii) the temporal two-step time-loop: one, highly variable, related to the flow changes, the other, slowly variable, related to the morphological changes. As a first step such an improvement could consist of incorporating a broader spectrum (FREILICH and GUZA, 1984).

LITERATURE CITED

BAGNOLD, R.A., 1963. Mechanics of marine sedimentation. *In:* HILL, M.N. (ed.), Volume 3. New York: Interscience, pp. 507–528.

BAILARD, J.A., 1981. An energetics total load sediment transport model for a plane sloping beach. *Journal of Geophysical Research*, 86, C6, 10938–10954.

BARENBLATT, G.F., 1953. On the motion of suspended particles in a turbulent stream. *Prikl. Mathem. Mekh.*, 17, 261–274.

BENDYKOWSKA, G., 1975. Quelques aspects de la transformation du profil de la houle en eau peu profonde. *Archiwum Hydrotechniki*, XXII, 97–103.

BHATTACHARYA, P.K. and KENNEDY, J.F., 1971. Sediment suspension in shoaling waves. *Proceedings of the 14th Congress IAHR*, 4, 137–144.

BOCZAR-KARAKIEWICZ, B., 1972. Transformation of wave profile in shallow water. Fourier analysis. *Archiwum Hydrotechniki*, XIX, 197–209.

BOCZAR-KARAKIEWICZ, B.; BONA, J.L., and COHEN, D.L., 1987. Interaction of shallow water wave and bottom topographies. *In:* BONA, J.L.; DAFERMOS, C.; ERICKSEN, J.L., and KINDERLEHRER, D., (eds.), *Dynamical Problems in Continuum Physics*. New York: Springer-Verlag, Vol. 4, pp. 131–176.

BOWEN, A.J. and INMAN, D.L., 1971. Edge waves and crescentic bars. *Journal of Geophysical Research*, 76, 8662–8671.

CARTER, T.G.; LIU, P.L.F. and MEI, C.C., 1973. Mass transport by waves and offshore sand bedforms. *Journal of Waterways, Harbour, Coastal Engineering*, 99, 165–184.

CHAPALAIN, G., 1988. Etude hydrodynamique et sédimentaire des environnements littoraux dominés par la houle. Thèse de Doctorat. de l'Université Joseph Fourier–Grenoble I. 318 p.

CHAPALAIN, G.; COINTE, R., and TEMPERVILLE, A.T., 1992. Observed and modeled resonantly progressive water-wave. *Coastal Engineering*, in press.

DAVIDSON-ARNOTT, R.G.D. and PEMBER, G.F., 1980. Morphology and sedimentology of multiple parallel bar systems, southern Georgian Bay, Ontario. *Journal of Great Lakes Research*, 6(3), 417–428.

DOWNING, J.P., 1984. Suspended sand transport on a dissipative beach. *Proceedings 19th International Conference Coastal Engineering*, pp. 1765–1781.

DYER, K.R., 1986. *Coastal and Estuarine Sediment Dynamics*. New York: Wiley.

FORBES, D.L.; FROBEL, D.; HEFFLER, D.E.; DICKIE, K., and SHIELS, C., 1986. Surficial geology, sediment mobility, and transport processes in the coastal zone at two sites in the southern Gulf of St. Lawrence: Pointe Sapin (N.B.) and Stanhope Lane (P.E.I.). *Canadian Coastal Sediment Study*, N.R.C., C2S2 Report 20.

FREILICH, M.H. and GUZA, R.T., 1984. Nonlinear effects on shoaling surface gravity waves. *Philosophical Transactions of the Royal Society of London*, A311, 1–41.

GALVIN, C.J., 1968. Shapes of unbroken, periodic gravity water waves. *Transactions of the American Geophysical Union*, 49, 206.

GIBBS, D.; MATTHEWS, M.D., and LINK, D.A., 1971. The relationship between sphere size and settling velocity. *Journal of Sedimentary Petrology*, 41(1), 7–78.

GODA, Y., 1967. Travelling secondary wave crests in wave channels. Appendix to: Laboratory investigation on wave transmission over breakwaters. *Japan Port and Harbours Research Institute*, N°13, 32–38.

GRANT, W.D. and MADSEN, O.S., 1982. Movable bed roughness in unsteady oscillatory flow. *Journal of Geophysical Research*, 87, C1, 469–481.

GRANT, W.D.; WILLIAMS III, A.J.; GLENN, S.M.; CACCHIONE, D.A., and DRAKE, D.E., 1983. High frequency bottom stress variability and its prediction in the CODE region. *WHOI report 83/19*, 72 p.

HANES, D.M., 1990. The structure of events of intermittent suspension of sand due to shoaling waves. *In:* LE MEHAUTE, B. and HANES, D.H. (eds.), *The Sea*, Volume 9, Ocean Engineering Science. New York: Wiley, pp. 941–952.

HANES, D.M. and HUNTLEY, D.A., 1986. Continuous measurements of suspended sand concentration in a wave dominated nearshore environment. *Continental Shelf Research*, 6(4), 585–596.

HANES, D.M.; VINCENT, C.E.; HUNTLEY, D.A., and CLARKE, T.L, 1988. Acoustic measurements of suspended sand concentration in the C2S2 experiment at Stanhope Lane, Prince Edward Island. *Marine Geology*, 81, 185–196.

HAYASHI, T. and OHASHI, M.A., 1983. A dynamical and visual study on the turbulent boundary layer. *In:* BRADBURY, R. (ed.), *Turbulent Shear Flows*. New York: Springer-Verlag, pp. 13–33.

HINO, M.; KASHIWAYANAGI, M.; NAKAYAMA, A., and HARA, T., 1983. Experiments on the turbulence statistics and the structure of a reciprocating oscillatory flow. *Journal of Fluid Mechanics*, 131, 363–399.

HORIKAWA, K., 1981. Coastal sediment processes. *Annual Review of Fluid Mechanics*, 13, 9–32.

HORIKAWA, K., 1988. *Nearshore Dynamics and Coastal Processes. Theory, Measurement, and Predictive Models*. Tokyo: University of Tokyo Press.

HUNT, J.N., 1954. The turbulent transport of suspended sediment in open channels. *Proceedings of the Royal Society of London*, A, pp. 322–335.

HUNT, J.N., 1969. On the turbulent transport of a heterogeneous sediment. *The Quarterly Journal of Mechanics and Applied Mathematics*, 22, 235–246.

INMAN, D.L. and BOWEN, A.J., 1962. Flume experiments on sand transport by waves and currents. *Proceedings of the 8th International Conference on Coastal Engineering*, pp. 137–150.

JOHNS, B., 1970. On the mass transport induced by oscillatory flow in a turbulent boundary layer. *Journal of Fluid Mechanics*, 43, 1, 177–185.

JONSSON, I.G., 1963. Measurements in the turbulent wave boundary layer. *Proceedings of the 10th Congress of the IAHR* (London), Vol. 1, pp. 85–92.

JONSSON, I.G., 1966. Wave boundary layers and friction factors. *Proceedings of the 10th International Conference on Coastal Engineering*, pp. 127–148.

JONSSON, I.G., 1978. A new approach to oscillatory rough turbulent boundary layers. Technical University of Denmark, Inst. of Hydrodynamics and Hydraulic Engineering. Ser. Pap. 17, p. 87. (Also published in *Ocean Engineering*, 1980, 7, 109–152.)

JONSSON, I.G. and CARLSEN, N.A., 1976. Experimental and theoretical investigations in an oscillatory turbulent boundary layer. *Journal of Hydraulic Research*, 14, 45–60.

JUSTESEN, P., 1988. Prediction of turbulent oscillatory flow over rough beds. *Coastal Engineering*, 12, 257–284.

KENNEDY, J.F. and LOCHER, F.A., 1972. Sediment suspension by water waves. *In:* Meyer, R.E,. (ed.), *Waves and Beaches*. New York: Academic, pp. 249–291.

LAMBRAKOS, K.F., 1982. Seabed wave boundary layer measurements and analysis. *Journal of Geophysical Research*, 87, C6, 4171–4189.

LAU, J. and BARCILON, V., 1972. Harmonic generation of shallow water waves over topography. *Journal of Physical Oceanography*, 2, 405–410.

LEWELLEN, W.S., 1977. Use of invariant modeling. *In:* FROST, W. (ed.), *Handbook of Turbulence*. Vol. 1. New York: Plenum, pp. 237–280.

LONGUET-HIGGINS, 1953. Mass transport in water waves. *Philosophical Transactions of the Royal Society of London*, A, 245, 535–591.

LUMLEY, J.L., 1978. Two-phase and Non-Newtonian flows. *In:* BRADSHAW, P. (ed.), *Topics in Applied Physics*. New York: Springer, Vol. 12, pp. 289–324.

MADSEN, O.S. and GRANT, W.D., 1976a. Sediment transport in coastal engineering. *M.I.T. Report 209*.

MADSEN, O.S. and GRANT, W.D., 1976b. Quantitative description of sediment transport by waves. *Proceedings of the 19th Conference on Coastal Engineering*, pp. 1093–1112.

MEI, C.C., 1983. *The Applied Dynamics of Ocean Surface Waves*. New York: Wiley.

MEI, C.C. and UNLUATA, U., 1972. Harmonic Generation in Shallow Water Waves. *In:* MEYER, R.E. (ed.), *Waves on Beaches*. New York: Academic, pp. 181–202.

NIELSEN, P., 1979. Some basic concepts of wave sediment transport. Technical University of Denmark, Institute of Hydrodynamics and Hydraulic Engineering, *Serial Paper 20*, 160p.

NIELSEN, P., 1988. Three simple models of wave sediment transport. *Coastal Engineering*, 12, 43–62.

NIELSEN, P.; GREEN, M.O., and COFFEY, F.C., 1982. Suspended sediment under waves. *Coastal Studies Unit Technical Report 82/6*.

PEREGRINE, D.G., 1972. Equations for water waves and the approximation behind them. *In:* MEYER, R.E. (ed.), *Waves on Beaches*. New York: Academic, pp. 95–121.

RAUDKIVI, A.J., 1976. *Loose Boundary Hydraulics*. New York: Pergamon.

RODI, W., 1980. Turbulence models and their application in hydraulics, State-of-the-Art paper presented by IAHR. 52 p.

RODI, W., 1987. Examples of calculation methods for flow and mixing in stratified fluids. *Journal of Geophysical Research*, 92, C5, 5305–5328.

ROUSE, H., 1937. Modern concepts of mechanics of turbulence. *Transactions of the American Society of Civil Engineering*, 102, 463–543.

SHENG, Y.P., 1984. A turbulent transport model of coastal processes. *Proceedings of the 19th International Conference on Coastal Engineering*, pp. 2380–2396.

SHENG, Y.P., 1985. A new one-dimensional ocean current model OCM1D. A.R.A.P. report prepared for Sohio Petroleum Company.

SHENG, Y.P., 1986. Modeling turbulent bottom boundary layer dynamics. *Proceedings of the 20th International Conference on Coastal Engineering*, pp. 1496–1508.

SHENG, Y.P. and VILLARET, C., 1989. Modeling the effects of suspended sediment stratification on bottom exchange processes. *Journal of Geophysical Research*, 94, C10, 14429–14444.

SHIBAYAMA, Y. and HORIKAWA, K., 1982. Sediment transport and beach transformation. *Proceedings of the 18th International Conference on Coastal Engineering,* pp. 1439–1458.
SHIELS, C.A., 1986. Geomorphological changes along the central north coast of Prince Edward Island, 1935–1985. B.A. Dissertation. St Mary's University. Halifax. 88 p.
SLEATH, J.F.A., 1987. Turbulent oscillatory flow over rough beds. *Journal of Fluid Mechanics,* 182, 369–409.
SMITH, J.D. and McLEAN, S.R., 1977. Spatially averaged flow over a wavy surface. *Journal of Geophysical Research,* 82, C12, 1735–1746.
SUMER, B.M.; JENSEN, B.L., and FREDSOE, J., 1987. Turbulence in oscillatory boundary layers. *In:* COMTE-BELLOT, G. and MATHIEU, J. (eds.), *Advances in Turbulence.* New York: Springer-Verlag, pp. 556–567.
SUNAMURA, T., 1980. A laboratory study of offshore transport of sediment and a model for eroding beaches. *Proceedings of the 17th International Conference on Coastal Engineering,* pp. 1051–1070.
SVENDSEN, I.A., 1977. A model of sediment motion under waves. Internal Research Note, Technical University of Denmark, Institute of Hydrodynamics and Hydraulic Engineering.
SVENDSEN, I.A. and LORENZ, R.Z., 1989. Three-dimensional velocity profile in combined undertow and longshore currents. *Coastal Engineering,* 13, 55–79.
VILLARET, C., 1987. Etude expérimentale et numérique des lois d'érosion pour des sédiments cohésifs. Thèse de Doctorat. l'Université Scientifique, Technologique et Médicale de Grenoble. 162 p.
VINCENT, C.E.; HANES, D.M., and BOWEN, A.J., 1991. Acoustic measurements of suspended sand on the shoreface and the control of concentration by bed roughness. *Marine Geology,* 96, 1–18.

APPENDIX A

"QUASI-EQUILIBRIUM" SECOND-ORDER TURBULENCE CLOSURE EQUATIONS

Equations completing the description of the sediment-laden flow in the boundary layer ((1), (2), and (3)) and relating the turbulent kinetic energy $q^2/2$ and the turbulent macroscale Λ are the following (SHENG, 1985, 1986; SHENG and VILLARET, 1989)

$$\frac{\partial q^2}{\partial t} = 2\nu_t\left(\frac{\partial u}{\partial z}\right)^2 - b\frac{q^3}{\Lambda} + v_c\frac{\partial}{\partial z}\left(q^2\frac{\partial q^2}{\partial z}\right) + 2\frac{\gamma_t g}{\rho_f}\frac{\partial \rho}{\partial z} \qquad (A.1)$$

$$\frac{\partial \Lambda}{\partial t} = -S_1\frac{\Lambda}{q^2}\nu_t\left(\frac{\partial u}{\partial z}\right)^2 + S_2 q + v_c\frac{\partial\left(q\Lambda\frac{\partial \Lambda}{\partial z}\right)}{\partial z} + \frac{S_4}{q}\left(\frac{\partial \Lambda q}{\partial z}\right)^2 - S_5 g\frac{\Lambda}{q^2}\frac{\gamma_t}{\rho_f}\frac{\partial \rho}{\partial z} \qquad (A.2)$$

where b, v_c, S_1, S_2, S_4 and S_5 are new experimentally determined constants respectively equal to 0.125, 0.3, 0.35, 0.6b, −0.375, −0.8 (LEWELLEN, 1977). Note that all constants in the present analysis are assumed to be invariant.

Analytical expressions for the eddy viscosity ν_t and for the eddy diffusivity γ_t are (VILLARET, 1987; CHAPALAIN, 1988)

$$\nu_t = \frac{1}{4}\frac{\Lambda q\left[1 + \left(\frac{1}{A} - \frac{1}{bs}\right)OM\right]}{\left[1 - 2\left(1 + \frac{1}{2bs}\right)OM\right](1 - OM)} \qquad (A.3)$$

$$\gamma_t = -\frac{1}{3}\frac{\Lambda q}{\left(2 + \frac{1}{bs} - \frac{1}{OM}\right)OM} \qquad (A.4)$$

where

$$OM = \frac{g\Lambda^2}{A\rho_t q^2}\frac{\partial \rho}{\partial z}$$

APPENDIX B

RIPPLE CHARACTERISTICS AND WAVE-INDUCED UPWARD FLUX OF SEDIMENT OVER A RIPPLED BED

Ripple characteristics are estimated for the equilibrium and breakup phases of the fluid motion (GRANT and MADSEN, 1982) according to quantitative criteria defined in Table 1. In Table 1, h_r is the ripple height, λ is the ripple wavelength and $a_0 = U_e/\omega_t$ is half the near-bed orbital excursion where U_e is the equivalent orbital velocity defined as

$$U_e = \left(\sum_j U_{bj}^2\right)^{1/2} \qquad (B.1)$$

where U_{bj} is the jth harmonic component of the velocity at the top of the bottom boundary layer. The expression of this quantity depends on the surface wave model. The expression for the Boussinesq model is given by (31).

Notations ψ' and ψ'_c are respectively MADSEN and GRANT's (1976a,b) wave-extended Shields parameter and its critical value. This parameter is defined by

$$\Psi' = 0.5\ f'_w U_c^2 \Big/ \left(\frac{\rho_s - \rho_f}{\rho_f}\right) gd \qquad (B.2)$$

where ρ_f and ρ_s are respectively the fluid and the sediment density, d is the sediment particle diameter, and f'_w is the Jonsson skin friction factor. S* is a parameter defined as

$$S_* = \frac{d}{4\nu}\sqrt{\left(\frac{\rho_s}{\rho_f} - 1\right) gd} \qquad (B.3)$$

where ν is the cinematical water viscosity. ψ'_c is determined by using GRANT and MADSEN's (1982) empirical results.

The wave-induced upward flux of sediment above a rippled bed is described by the time-periodic pick-up function (SVENDSEN, 1977; NIELSEN, 1979) characterized by two peaks located at the free velocity reversals (*i.e.*, phases when the vortices are released in the bottom boundary layer, Figure 21) and expressed as

$$p(t) = p_o + \frac{p_o}{1+\mu}\sum_{n=1}^{m}\frac{2(m!)^2}{(m+n)!(m-n)!} \cdot \left|\cos n(\omega_1 t - \Phi^+) + \mu \cos n(\omega_1 t - \Phi^-)\right| \qquad (B.4)$$

where the parameter $\mu = [U_b^{-2}]/[U_b^{+2}]$ allows an account of nonlinearities of the wave field. In (B.4) m is a parameter controlling the skewness of the peaks, superscripts + and − refer to the phases (Φ^+, Φ^-) of the velocity reverse following the maximum and the minimum outer flow velocity respectively (Figure 21). The quantity denoted by p_0 is equal to $\bar{C} \cdot w_f$ where w_f is the sediment fall velocity which can be determined as a function of the particle diameter d, the fluid dynamic viscosity μ_f, the fluid density ρ_f, and the sediment density ρ_s (expressed in cgs unit system) by the expression of GIBBS *et al.* (1971)

$$w_f = \frac{-3\mu_f + \sqrt{9\mu_f + 0.25gd^2\rho_f(\rho_s - \rho_f) \cdot (0.0155 + 0.0992d)}}{\rho_f(0.01161 - 0.0774d)} \qquad (B.5)$$

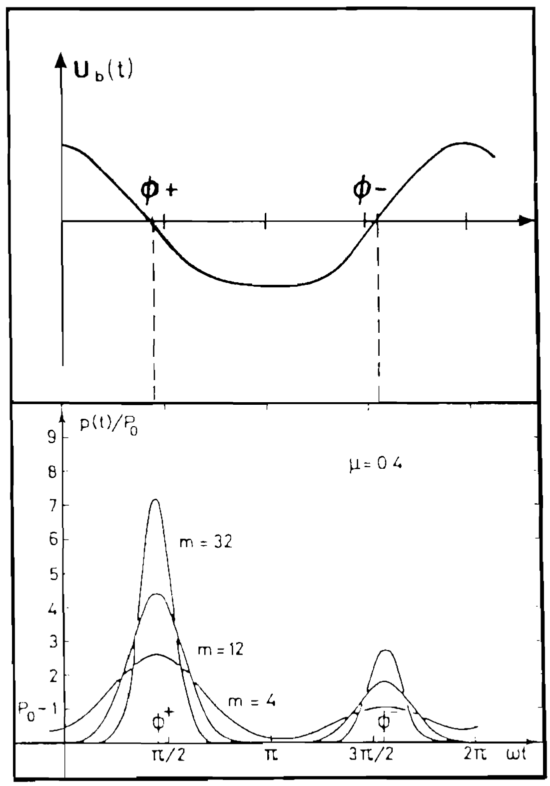

Figure 21. Near-bed "driving" velocity U_b and Svendsen-Nielsen's pickup function p(t).

$\bar{C}_0$ is the mean bottom concentration is given by NIELSEN (1979) as

$$\bar{C}_0 = 0.028(\Psi' - \Psi'_c)\frac{2}{\pi} - \arcos\left(\frac{\Psi'_c}{\Psi'}\right)^{1/2} \qquad (B.6)$$

This expression was obtained above a crest. A smaller value for the constant was found above a trough. A spatial average would be somewhere between the two expressions, but on account of the many simplifications assumed during the preceding developments the expression for the crest mean bottom concentration is adopted.

APPENDIX C

WAVE-INDUCED VELOCITIES, SEDIMENT CONCENTRATION AND RELATED SEDIMENT TRANSPORT RATES IN A NEAR-BED BOUNDARY LAYER

The first-order oscillatory velocity component is given by

$$U = \alpha u^{(1)} = \alpha \mathrm{Re} \sum_{j=1}^{2} U_j \exp[-(1+i)\eta_j] \quad \text{(C.1)}$$

where

$$\eta_j = z/l_j = z \Big/ \sqrt{\frac{2\nu_t}{\omega_j}}$$

On account of the smallness of the imaginary part of the wave number k_j^{+I} in geophysical conditions (CHAPALAIN, 1988) the second-order steady velocity, identified with the mass transport velocity (LONGUET-HIGGINS, 1953), may be approximated by

$$u_s = \frac{\alpha^2\beta}{4} \sum_{j=1}^{2} \left| 1 - \frac{1}{6}\beta^2 k_j^{R2} h^2 \right|^2$$

$$\cdot \frac{\omega_j}{k_j^R} |a_j|^2 \exp\left(\frac{2k_j^I}{\beta}\right) H_j^I(\eta_j) \quad \text{(C.2)}$$

where

$$H_j^I = -8\exp(-\eta_j)\cdot\cos\eta_j + 3\exp(-2\eta_j) + 5 \quad \text{(C.3)}$$

The expression for spatial and temporal evolution of the suspended sediment concentration is

$$c(X,z,t) = \sum_n \frac{\bar{C}_0}{1+\mu} \cdot \frac{a'_n}{\alpha_n}$$

$$\cdot (\exp(-in\Phi^+) + \mu \exp(-in\Phi^-))$$

$$\cdot \exp\left(-\frac{w_f}{\gamma_t}\alpha_n z\right) \exp(in\omega_1 t) \quad \text{(C.4)}$$

where

$$a'_n = \frac{2(m!)^2}{(m+n)!(m-n)!}$$

and

$$\alpha_n = \frac{1}{2} + \sqrt{\frac{1}{4} + i\frac{n\omega\gamma_t}{w_f^2}}$$

The definitions of Φ^+, Φ^-, $\bar{C}_0$ and μ are given in Appendix B.

The time-independent sediment transport rate Q_m is

$$Q_m(X) = \frac{1}{4}\alpha^2\beta\bar{C}_0(X) \sum_{j=1}^{2} \frac{-8\delta_j}{(D\delta_j - 1)^2 + 1}$$

$$\cdot [\exp(D\delta_j - 1)\eta_{sj}$$

$$\cdot ((D\delta_j - 1)\cos\eta_{sj} + \sin\eta_{sj}) + 1]$$

$$+ \frac{3\delta_j}{D\delta_j - 2} \exp[(D\delta_j - 2)\eta_{sj}]$$

$$+ \frac{5}{D}\exp[-D\eta_{sj}] \quad \text{(C.5)}$$

The time-dependent sediment contribution Q_n in an integral form is

$$Q_n(X) = \frac{S}{2}\mathrm{Re}\left\{ \sum_{j=1}^{2} \frac{\bar{C}_0}{(1+\mu)\alpha_j} U_j a'_j \right.$$

$$\cdot (\exp(-ij\Phi^+) + \mu\exp(-ij\Phi^-))$$

$$\cdot \int_0^\delta \exp\left(\frac{-w_f\alpha_j z}{\gamma_t}\right)$$

$$\left. \cdot (1 - \exp(-(1-i)\beta_j z))\, dz \right\} \quad \text{(C.6)}$$

where $\beta_j = 1/\delta_j$, $\eta_{sj} = \delta/\delta_j$ and which after some algebraic manipulations becomes

$$Q_n(X) = \frac{S_0 C_0}{2(1+\mu)} \sum_{j=1}^{2} a'_j \frac{\gamma_t}{w_f|\alpha_j|^2}$$

$$\cdot \left[\{A_j\alpha_j^{+R} - B_j\alpha_j^I\} e^{\frac{w_f\alpha_j^R\delta}{\gamma_t}} (A_jE_j - B_jF_j) \right]$$

$$+ \frac{a'_j}{\left(\frac{w_f\alpha_j^R}{\gamma_t} + \beta_j\right)^2 + \left(\frac{w_f\alpha_j^I}{\gamma_t} - \beta_j\right)^2}$$

$$\cdot \left[-A_j\left(\frac{w_f\alpha_j^R}{\gamma_t} + \beta_j\right) + \beta_j\left(\frac{w_f\alpha_j^I}{\gamma_t} - \beta_j\right) \right]$$

$$+ e^{\left(\frac{w_f}{\gamma_t}\alpha_j^R + \beta_j\right)\delta} \cdot (A_jG_j - B_jH_j) \quad \text{(C.7)}$$

where:

$$A_j = \frac{1}{|\alpha_j|^2}[C_j\cdot(U_j^R\alpha_j^R - U_j^I\alpha_j^I)$$

$$- S_j\cdot(U_j^I\alpha_j^R + U_j^R\alpha_j^I)] \quad \text{(C.8)}$$

$$B_j = \frac{1}{|\alpha_j|^2}\cdot[S_j\cdot(U_j^R\alpha_j^R - U_j^I\alpha_j^I)$$

$$+ C_j\cdot(U_j^I\alpha_j^R + U_j^R\alpha_j^I)] \quad \text{(C.9)}$$

$$E_j = \alpha_j^R \cos\left(\frac{w_f}{\gamma_t}\alpha_j^I\delta\right) - \alpha_j^I \sin\left(\frac{w_f}{\gamma_t}\alpha_j^I\delta\right) \quad \text{(C.10)}$$

$$F_j = \alpha_j^I \cos\left(\frac{w_f}{\gamma_t}\alpha_j^I \delta\right) + \alpha_j^R \sin\left(\frac{w_f}{\gamma_t}\alpha_j^I \delta\right) \qquad (C.11)$$

$$G_j = \left(\frac{w_f \alpha_j^R}{\gamma_t} + \beta_j\right)\cdot\cos\left[\left(\frac{w_f \alpha_j^I}{\gamma_t} - \beta_j\right)\delta\right]$$

$$- \left(\frac{w_f \alpha_j^I}{\gamma_t} - \beta_j\right)\cdot\sin\left[\left(\frac{w_f \alpha_j^I}{\gamma_t} - \beta_j\right)\delta\right] \qquad (C.12)$$

$$H_j = \left(\frac{w_f \alpha_j^R}{\gamma_t} + \beta_j\right)\cdot\sin\left[\left(\frac{w_f \alpha_j^I}{\gamma_t} - \beta_j\right)\delta\right]$$

$$+ \left(\frac{w_f \alpha_j^I}{\gamma_t} - \beta_j\right)\cdot\cos\left[\left(\frac{w_f \alpha_j^I}{\gamma_t} - \beta_j\right)\delta\right] \qquad (C.13)$$

with

$$C_j = \cos(j\Phi') + \mu\cdot\cos(j\Phi) \qquad (C.14)$$
$$S_j = \sin(j\Phi') + \mu\cdot\sin(j\Phi) \qquad (C.15)$$

We recall that superscripts R and I denote respectively the real and the imaginary part of the considered variable.

APPENDIX D

COEFFICIENTS OF THE NONLINEAR AMPLITUDE EQUATIONS

The two coefficients H_j ($j = 1,2$)

$$H_j = \frac{1}{f}\,\frac{k'_j\left(1 + \frac{2}{3}\omega_j^2\right)}{2\left(1 - \frac{1}{3}\omega_j^2\right)} \qquad j = 1, 2 \qquad (D.1)$$

represent the influence of the bottom topography on the wave train. The remaining two coefficients $S_i(j = 1, 2)$

$$S_1 = \frac{\omega_1^2\omega_2\left(\frac{1}{k'_1} - \frac{1}{k'_2}\right) + \left(\frac{\omega_1}{k'_1} - \frac{\omega_2}{k'_2}\right)(k'_2 - k'_1)}{4\left(1 - \frac{1}{3}\omega_1^2\right)} \qquad (D.2)$$

and

$$S_2 = \frac{(\omega_1 - (2k'_1)^2)}{2\,k'_2\left(1 - \frac{1}{3}\omega_2^2\right)} \qquad (D.3)$$

represent the effect of nonlinear interaction between the harmonic components of the surface wave.

□ RESUMEN □

Este trabajo presenta un modelo numérico realizado para examinar la hidrodinámica y los procesos sedimentarios relacionados con olas progresivas, propagándose en áreas cercanas a la costa, cuando aún no se ha producido la rotura de la ola. La primera parte del trabajo concierne a los procesos de microescala que se desarrollan en la cercania de la capa límite del fondo. Durante la primera etapa del estudio se aplicó un modelo de segundo orden. El modelo numérico fue contrastado con datos experimentales y se lo aplicó a la predicción del flujo sedimentario en suspensión cercano al fondo, e inducido por olas lineales y no lineales. Para ambientes costeros con régimen de olas normales y con bajas concentraciones volumétricas de sedimentos ($c = 10^{-3}$ 10^{-4}) el modelo predice una débil influencia de las partículas de sedimento sobre las velocidades medias del flujo. Durante la segunda etapa del estudio, el procedimiento de modelación fue desacoplado, separando la dinámica del flujo a partir de la difusón y de la adveción del sedimento. Los resultados de un modelo analítico de clausura, más sencillo, fueron comparados contra los del modelo de segundo orden, hallándose una concordancia aceptable. La segunda parte del trabajo ha sido dedicada a los procesos costeros de macroescala. Un modelo analítico sencillo de la capa límite del fondo se incorporó al modelo bidimensional morfodinámico y de transporte de sedimento, del frente exterior de la zona costera dominada por la energía eólica de condiciones moderadas.—*Nestor W. Lanfredi, CIC-UNLP, La Plata, Argentina.*